Hematopoietic Transfer of the Anti-Cancer and Lifespan-Extending Capabilities of A Genetically Engineered Blood System

Jing-Ping Wang[#1,2], Chun-Hao Hung[#1,2*], Yao-Huei Liou[2,8], Ching-Chen Liu[2], Kun-Hai Yeh[2], Keh-Yang Wang[1,2], Zheng-Sheng Lai[2], Tzu-Chi Hsu[1,2], Tung-Liang Lee[2,6], Yu-Chiau Shyu[2,3,6*], Pei-Wen Hsiao[4,5], Liuh-Yow Chen[2], Trees-Juen Chuang[#,7], Chen-Hsin Albert Yu[2], Nah-Shih Liao[2], and Che-Kun James Shen[1,2*]

1. The PhD Program for Neural Regenerative Medicine, Taipei Medical University, Taipei 115, Taiwan
2. Institute of Molecular Biology, Academia Sinica, Nankang, Taipei 115, Taiwan
3. Department of Nursing, Chang Gung University of Science and Technology, Taoyuan City 333, Taiwan
4. Agricultural Biotechnology Research Center, Academia Sinica, Nankang, Taipei 115, Taiwan
5. Graduate Institute of Life Sciences, National Defense Medical Center, Taipei 115, Taiwan
6. Community Medicine Research Center, Chang Gung Memorial Hospital, Keelung Branch, Keelung 204, Taiwan
7. Genomics Research Center, Academia Sinica, Nankang, Taipei 115, Taiwan
8. Current address- Department of Molecular Metabolism, T.H. Clan School of Public Health, Harvard University, 677 Huntington Ave, Boston, MA 02115, USA

# Contributed equally

* Corresponding Authors

Please send all correspondence to:

Che-Kun James Shen
The PhD Program for Neural Regenerative Medicine
Taipei Medical University
Taipei 115, Taiwan, ROC
E-mail: ckshen@gate.sinica.edu.tw

Yu-Chiau Shyu
Community Medicine Research Center,
Chang Gung Memorial Hospital, Keelung Branch,
Keelung 204, Taiwan (R.O.C.)
E-mail: yuchiaushyu@gmail.com

Chun-Hao Hung
The PhD Program for Neural Regenerative Medicine
Taipei Medical University
Taipei 115, Taiwan, ROC
E-mail: libur777@hotmail.com

Abstract

A causal relationship exists among the aging process, organ decay and dis-function, and the occurrence of various diseases including cancer. A genetically engineered mouse model, termed *Eklf*$^{K74R/K74R}$ or *Eklf*(K74R), carrying mutation on the well-conserved sumoylation site of the hematopoietic transcription factor KLF1/ EKLF has been generated that possesses extended lifespan and healthy characteristics including cancer resistance. We show that the high anti-cancer capability of the *Eklf*(K74R) mice are gender-, age- and genetic background-independent. Significantly, the anti-cancer capability and extended lifespan characteristics of *Eklf*(K74R) mice could be transferred to wild-type mice via transplantation of their bone marrow mononuclear cells. Targeted/global gene expression profiling analysis has identified changes of the expression of specific proteins and cellular pathways in the leukocytes of the *Eklf*(K74R) that are in the directions of anti-cancer and/or anti-aging. This study demonstrates the feasibility of developing a novel hematopoietic/ blood system for long-term anti-cancer and, potentially, for anti-aging.

Introduction

Aging of animals, including humans, is accompanied by lifespan-dependent organ deterioration and the occurrence of chronic diseases such as cancer, diabetes, cardiovascular failure and neurodegeneration[1,2]. To extend healthspan and lifespan, various biomedical- and biotechnology-related strategies have been intensively developed and applied, including the therapy of different diseases such as cancer[3-5]. The hematopoietic/ blood system is an important biomedical target for anti-aging and anti-cancer research development. Multiple blood cell lineages arise from hematopoietic stem cells (HSCs), with the lymphoid lineage giving rise to T, B, and natural killer (NK) cell populations, whereas the myeloid lineage differentiates into megakaryocytes, erythrocytes, granulocytes, monocytes and macrophages[6-8]. The genetic constituents and homeostasis of the hematopoietic system are regulated epigenetically and via environmental factors to maintain animal health[6,9].

EKLF, also named KLF1, is a Krüppel-like factor that is expressed in a range of blood cells including erythrocytes, megakaryocytes, T cells, NK cells, as well as in various hematopoietic progenitors including common-myeloid-progenitor, megakaryocyte-erythroid-progenitor (MEP), and granulocyte-macrophage-progenitor[10-12]. The factor regulates erythropoiesis[13] and the differentiation of MEP to megakaryocytes and erythrocytes[10,14] as well as of monocytes to macrophages[15]. EKLF is also expressed in HSC and regulates their differentiation[16]. The factor can positively or negatively regulate transcription through binding of its zinc finger domain to the CACCC motif of the regulatory regions of a diverse array of genes[16-19].

EKLF could be sumoylated *in vitro* and *in vivo*, and sumoylation of the lysine at codon 74 of mouse EKLF altered the transcriptional regulatory function[10] as well as nuclear import[20] of the factor. Surprisingly, homozygosity of a single amino acid substitution, lysine(K) to arginine(R), at the sumoylation site of EKLF results in the generation of a novel mouse model with healthy longevity. These mice, termed *Eklf*$^{K74R/K74R}$ or *Eklf*(K74R), exhibited extended healthspan and lifespan. In particular, the *Eklf*(K74R) mice showed delay of the age-dependent decline of physical performance, such as the motor function and spatial learning/memory capability, and deterioration of the structure/function of tissues including the heart, liver, and kidney. Furthermore, the *Eklf*(K74R) mice appeared to have significantly higher anti-cancer capability than the WT mice[21].

As described in the following, we have since characterized the high anti-cancer capability of the *Eklf*(K74R) mice with respect to its dependence on the age, gender and genetic background. More importantly, we have demonstrated that the high anti-cancer ability of these genetically engineered mice could be transferred to wild type mice (WT) through hematopoietic transplantation of the bone marrow mononuclear cells (BMMNC). Furthermore, we show that the higher anti-cancer capability and extended life span of *Eklf*(K74R) mice are associated with changes of the global protein expression profile and specific aging-/cancer-associated cellular signaling pathways in their white blood cells (WBC), or leukocytes.

Result

Characterization of the cancer resistance of *Eklf*(K74R) mice in relation to age, gender, and genetic background

The *Eklf*(K74R) mice appeared to be cancer resistant to carcinogenesis as manifested by their lower spontaneous cancer incidence (12.5%) in life than WT mice (75%). The *Eklf*(K74R) mutation also protected the mice from metastasis in the experimental metastasis assay and it reduced tumor growth in the subcutaneous cancer cell inoculation assay[21]. We have used the pulmonary melanoma foci assay to further characterize the higher cancer resistance of the *Eklf*(K74R) mice with respect to the effects of gender/age/genetic background of the mice and the requirement of the homozygous K74R mutation.

It appeared that male as well as female *Eklf*(K74R) mice in the B6 genetic background had significantly fewer pulmonary melanoma foci than the corresponding WT mice (Figure 1). Because of this result, we used male mice for all of the studies describe below. First, both young (2-month-old) and aged (24-month-old) *Eklf*(K74R) mice had higher anti-metastasis ability against the injected melanoma cells than WT mice of age-dependent groups (Figure 1A and 1B). Secondly, homozygosity of the K74R substitution was required for the higher cancer resistance of the *Eklf*(K74R) mice (Figure S1). Consistent with the previous study[21], the *Eklf*(K74R) mice survived longer than the WT mice after the injection of B16-F10 cells. Importantly, the *Eklf*(K74R) mice in the FVB background also exhibited high cancer resistance than FVB WT mice by this assay (Figure 1C), suggesting that cancer resistance of *Eklf*(K74R) mice conferred by the homozygous K74R substitution was likely genetic background-independent. Finally, the higher anti-cancer capability of the *Eklf*(K74R) mice

did not appear to depend on the arginine at codon 74, since *Eklf*(K74A) mice carrying K→A amino acid substitution at the K74 sumoylation site also exhibited higher anti-metastasis capability than WT mice in the pulmonary foci assay (Figure 1D).

Transfer of the anti-cancer capability and extended lifespan of *Eklf*(K74R) mice to WT mice via BMT

Since EKLF is a hematopoietic transcription factor expressed not only in mature blood cells but also in HSCs and hematopoietic stem progenitor cells, this cancer resistance may be transferable by means of BMT. This possibility was tested with uses of male mice and a standard BMT protocol[22]. BMMNC were purified from the bone marrow of 2-month-old CD45.2 *Eklf*(K74R) or WT mice and injected into the tail vein of CD45.1 WT recipient mice. Blood replacement of recipient mice with 10Gy γ-irradiation by that of the donor mice reached 90% at 7th-week (Figure 2A and 2B). After 2 weeks, the recipient mice were injected with B16-F10 cells and then sacrificed a further 2 weeks later to quantify pulmonary tumor foci. We found that WT mice transplanted with WT BMMNC had similarly high numbers of tumor foci relative to WT mice without BMT (Figure 2C and 1A). However, similar to *Eklf*(K74R) mice challenged with B16-F10 cells (Figure 1B), WT mice that received BMMNC from *Eklf*(K74R) mice presented significantly fewer tumor foci on their lungs (Figure 2C). Notably, BMT using 24-month-old donor mice gave similar result (Figure S2A).

In order to determine if WT mice having more restricted blood replacement upon BMT from *Eklf*(K74R) mice still exhibited a higher anti-cancer capability, we also carried out BMT experiments with lower doses of γ-irradiation. BMT using two lower doses of γ-irradiation (2.5Gy/5Gy) still resulted in transfer of cancer resistance from *Eklf*(K74R) to WT mice. Approximately 40% of recipient blood cells were substituted by donor cells upon BMT with 5Gy γ-irradiation. Consequently, at that irradiation dosage, BMT from *Eklf*(K74R) mouse donors reduced the average number of pulmonary tumor foci in recipient WT mice to 5. On the other hand, only 20% blood replacement was achieved in the recipient mice with 2.5Gy γ-irradiation (Figure 2D). However, the WT mice receiving BMT from *Eklf*(K74R) mice again developed less number (~10/mouse) of pulmonary tumor foci than those WT mice receiving BMT from the WT mice (Figure 2D). Thus, even at a low level of 20% blood replacement, BMT still enabled effective transfer of cancer resistance from *Eklf*(K74R) mice to WT mice.

In addition, we also attempted to transfer the extended lifespan characteristics of the *Eklf*(K74R) mice to WT mice by BMT. Significantly, the medium lifespan of WT mice

receiving BMT from *Eklf*(K74R) mice was 5 months longer than that of WT mice receiving BMT from WT mice (Figure S2B). Thus, the longer lifespan characteristics of the *Eklf*(K74R) mice was also transferable via BMT.

Inhibition of tumor growth by transplanted BMMNC from *Eklf* K74R) mice

Our experiments indicated that *Eklf*(K74R) bone marrow carried the anti-metastasis capability that prevented melanoma cell colonization on the lungs of recipient mice (Figures. 1 and 2). To determine if *Eklf*(K74R) BMT could inhibit tumor growth, we examined the effect of BMT on growth of tumors with B16-F10-luc cells. As outlined in Figure 3A, ten days after injection of cancerous cells, the formation of bioluminescent signals in the recipient mice were confirmed by the observation of *in vivo* bioluminescence. The following day, we transplanted the recipient mice with BMMNC from WT or *Eklf*(K74R) mice and then measured the intensities of bioluminescence signals from tumors 7 and 14 days later. As shown, tumor growth in mice subjected to BMT from *Eklf*(K74R) mice was significantly slower relative to those receiving BMMNC from WT mice (Figure 3B and 3C). Thus, *Eklf*(K74R) BMMNC indeed can inhibit the growth of tumor more effectively than WT BMMNC.

Differential expression of specific immune-, ageing- and/or cancer- associated biomolecules in the blood of *Eklf*(K74R) mice

The K74R substitution did not alter the expression levels of EKLF in the bone marrow, fetal liver[21] and the PB cells (Figure S1D), neither did it affect much the PB populations as shown by CBC analysis[21]. We further analyzed the PB populations by flow cytometry of WT and *Eklf*(K74R) mice of the ages 3 and 24 months, respectively. The frequency of *Eklf*(K74R) $NK1.1^+$ cells were higher than WT $NK1.1^+$ cells at aged mice. The latter observation correlated with the finding by Shyu *et al.* that the NKT cells in PB cells of 24-month-old *Eklf*(K74R) mice was higher than that of 24-month-old WT mice (Figure S3).

We first used RT-qPCR to analyze the levels in PB cells of mRNAs encoding the immune checkpoint genes (ICGs) PD-1/PD-L1[23] in view of the cancer resistance of *Eklf*(K74R) mice (Figure 4) as well as increased levels of PD-1 and PD-L1 in aged or tumorigenic mice[24]. As shown in Figure 4, the mRNA levels of *Pd-1* and *Pd-l1* in the PB, B cells and T cells of WT mice were both increased during aging. In great contrast, the mRNA levels and protein levels of these two genes were lower in 3-month-old *Eklf*(K74R) mice than the age-matched WT mice, and they remained low during ageing of the *Eklf*(K74R) mice.

Importantly, EKLF positively regulated expression of both *Pd-1* and *Pd-l1* at the transcriptional level, as demonstrated by RNAi knockdown experiments in splenic $CD3^+$ T cells (Figure 4C). As expected, lower levels of *Pd-1* and *Pd-11* expression were also observed in the PB of mice receiving BMT from *Eklf*(K74R) mice (Figure S2C). These findings indicate that the low tumorigenesis rate of *Eklf*(K74R) mice arises in part from low expression of the ICGs, *Pd-1* and *Pd-l1*.

We have also examined, by bead-based multiplex assay[25,26], the expression patterns of several ageing- and/or cancer- associated cytokines. As shown in Figure S4, there was no significant difference in the serum levels of IL-1β, IL-2, IL-10, IL-12p70, INF-γ or TNF-α between WT and *Eklf*(K74R) mice at 24-month-old. In contrast, the level of IL-4, an anti-inflammatory cytokine[27] beneficial to the hippocampus of aging mice[28], in 24-month-old *Eklf*(K74R) mice was 3-4 fold higher than the 24-month-old WT mice. On the other hand, the level of IL-6, a key factor in chronic inflammatory diseases, autoimmunity, cytokine storm and cancer[26,29], increased only moderately during aging of the *Eklf*(K74R) mice (Figure S4). Thus, similar to PD-1 and PD-L1, the altered expression of some of the cytokines in the blood likely contributes to the anti-aging and/or anti-cancer characteristics of the *Eklf*(K74R) mice.

Comparative proteomics analysis of the leukocytes of *Eklf*(K74R) mice and WT mice

We proceeded to examine age-dependent cell-intrinsic changes in the proteomes of the leukocytes from the WT and *Eklf*(K74R) mice in two different age groups. 259 and 306 differentially expressed proteins (DEPs) were identified between the two age groups for the WT and *Eklf*(K74R) mice, respectively (Figure S5A). To understand the correlations of these proteins with aging and cancer, we performed the GSEA and found that the age-dependent DEPs changed in the concordant direction in the WT and *Eklf*(K74R) mice were enriched for several known aging-related pathways, e.g. IL-6-JAK-STAT3 signaling, DNA repair, etc[30] (Figure S5B). Meanwhile, the age-dependent DEPs changed in the reverse directions in the WT and *Eklf*(K74R) mice were enriched for nine other aging-related pathways (Figure S5C).

We further performed DEP analyses between WT and *Eklf*(K74R) mice and identified strain-dependent DEPs in the two age groups. As shown in Figure S5D, only 7 DEPs were identified in the 3-month-old mice but 40 DEPs in the 24-month-old ones. Of the 40 DEPs in the elder mice, 3 and 37 were upregulated in *Eklf*(K74R) and WT mice, respectively (Figure S4D). Significantly, GSEA analysis of these DEPs showed that elder *Eklf*(K74R) leukocytes were enriched for the anti-aging pathways related to hypoxia, and p53 signaling, etc.[31,32], while the elder WT leukocytes were enriched for the aging-associated pathways related to

apoptosis, and mTORC1 signaling, etc[31,33]. On the other hand, the DEPs in elder *Eklf*(K74R) leukocytes were also enriched for anti-cancer pathways related to the interferon-α response, and TGF-β signaling, etc.[34-36] (Figure S5E), while DEPs in the elder WT leukocytes were enriched for the pro-cancer pathways related to IL-6-JAK-STAT3 signaling and angiogenesis[37]. These data together have demonstrated that *Eklf*(K74R) leukocytes contribute to their anti-cancer capability and long lifespan through several specific cellular signaling pathways.

Discussion

Because of the complexity and intercrosses of the different pathways regulating the health and the aging process, genetic manipulation of non-human animals[38,39] and non-genetic approaches on animals including human[4,40,41] targeting these pathways inevitably lead to moderate-to-severe side effects such as body weight loss, adiposity, etc.. With respect to the above, the *Eklf*(K74R) mice[21] is ideal as an animal model for further insightful understanding of the ageing process as well as for biomedical development of new anti-ageing tools and approaches. Indeed, the studies reported above on the hematopoietic transfer of the anti-cancer capability and extended lifespan of *Eklf*(K74R) mice have demonstrated the feasibility of a novel hematopoietic blood system for anti-disease and anti-ageing.

The anti-cancer capability of the *Eklf*(K74R) mice have rendered them relatively free from spontaneous cancer occurrence[21], which is also reflected by their resistance to tumorigenesis of the B16-F10 cells and LLC1 cells in the cancer-growth inhibition assay[21] (Figures. 1 and 3). Furthermore, the cancer resistance of *Eklf*(K74R) mice appears to be independent of the gender, age, and genetic background (Figure 1). The anti-metastasis property of the *Eklf*(K74A) mice in the pulmonary foci assay (Figure 1D) also indicates that the anti-cancer capability of the *Eklf*(K74R) mice is not due to the structural and/or post-translational properties of the arginine introduced at codon 74 of EKLF. Importantly, we have shown that the anti-cancer capability and the extended lifespan characteristics of *Eklf*(K74R) mice are transferrable through BMT (Figures. 2, 3, and S2B). In particular, we show that BMMNC from *Eklf*(K74R) mice (Figure 2A and S2A) could confer 2-month-old WT recipient mice with the anti-cancer capability. Furthermore, ~20% of blood substitution would allow the recipient mice to become cancer resistant in the pulmonary foci assay (Figure 2D). Also, WT mice receiving BMMNC at 2-month-old *Eklf*(K74R) mice would live longer than those receiving WT BMMNC (Figure S2B). In interesting parallel, infusion of HSC(K74R) could extend the life span of aged WT recipient mice[21]. Hematopoietic stem cell

therapy for different diseases[42-45] including cancer has been intensively explored and practiced such as leukemia, and neuroblastoma, etc[46,47]. Also, certain characteristics of the young mice could be transferred to old mice via heterochronic parabiosis or heterochronic transplantation[48-51]. Similarly, plasma proteins from human umbilical cord blood can revitalize hippocampal function and neuroplasticity in aged mice[52,53]. Thus, transplantation/transfer of the blood MNC carrying homozygous mutation at the sumoylation site of EKLF could be developed as a new approach for anti-cancer cell, long-term anti-aging and rejuvenation.

The tumorigenesis resistance and long lifespan exhibited by the *Eklf*(K74R) mice are most likely due to changes in the transcription regulatory properties of the mutant EKLF(K74R) protein relative to WT[54]. As exemplified in Figure 4A and 4B, expression levels of the ICGs *Pd-1* and *Pd-l1* in the PB, B, and T cells of *Eklf*(K74R) mice are reduced in comparison to the WT mice. Notably, cancer incidence increases with aging[55], which is accompanied by increased expression of PD-1 and PD-L1[56]. The lower expression of ICGs would contribute to the anti-cancer capabilities of the *Eklf*(K74R) blood to fight against cancer (Figures. 1, 2, and 3) and to extension of the lifespan of cancer-bearing mice[21]. Given that EKLF is expressed in HSCs[16], B cells, T cells[12], NK cells and macrophages (bio-GPS database), and that RNAi knockdown of *Eklf* expression significantly reduced *Pd-1* and *Pd-l1* mRNA levels in splenic $CD3^+$ T cells (Figure 4C), we assert that this protein is an upstream transcriptional regulator of the *Pd-1* and *Pd-l1* genes and, more generally, it regulates the transcriptomes of a diverse range of hematopoietic cells. Indeed, similar to ICGs, the expression levels of several cytokines in the *Eklf*(K74R) blood/serum are also different from the WT blood and some of the changes during ageing or carcinogenesis in the *Eklf*(K74R) blood are opposite to the blood/serum of WT mice [26] (Figure S4).

Previously, the transcriptome data have been used to dissect the regulation of leukocyte aging [30,57,58]. In addition, proteomic analysis has revealed the signaling pathways that regulate aging of specific types of leukocyte such as the lymphocyte and neutrophils cells[59,60]. In this study, we have performed proteomics analysis of leukocytes from WT and *Eklf*(K74R) mice in two age groups, and found that for the elder mice, the strain-dependent DEPs in the leukocytes are enriched for a number of signaling pathways. Among these signaling pathways, at least 12 of them are closely associated with the aging process, which include hypoxia, DNA repair, etc. (Figure S5E). As summarized by the model in Figure S5F, it appears that changes of these pathways in the elder *Eklf*(K74R) leukocytes relative to the elder WT leukocytes are mostly in the direction of anti-aging. The data of Figure S4 together strongly

suggest that the *Eklf*(K74R) amino acid substitution causes a change in the global gene expression profile of the leukocytes, which contributes to the high anti-cancer capability and long lifespan of the *Eklf*(K74R) mice.

In sum, we have characterized the cancer resistance of the *Eklf*(K74R) mice, among their other healthy characteristics, in relation to gender, age, and genetic background. We also have identified cell populations, gene expression profiles and cellular signaling pathways of the white blood cells of young and old mutant mice, in comparison to the WT ones, that are changed in the anti-cancer and/or anti-ageing directions. Finally, the transferability of the cancer resistance and extended life-span of the mutant mice via transplantation of BMMNC suggests the possibility of future development of hematopoietic blood cells genome-edited at the conserved sumoylation site of EKLF for anti-cancer and the extension of healthspan and/or lifespan in animals including human.

Acknowledgments

We thank Ya-Min Lin and her colleagues at the FACS Core for their efforts on the cell sorting. We also thank Taiwan Mouse Clinic facility for expertise help on the IVIS experiments. The effort by Dr. Ching-Yen Tsai at the Transgenic Core Facility, IMB, is greatly appreciated. The Immune Monitoring Core of Taipei Medical University provided great help in the analysis of the blood cell populations. We also thank the Bioinformatics Core Facility, IMB, for its efforts on the proteomics analysis.

Competing interests

The authors declare there is no conflict of interest.

Animal

All the animal procedures were approved by the Institute of Animal Care and Use Committees, IACUC, at Academia Sinica. The IACUC numbers are 17-02-1052, 17-12-1142, 20-10-1528, BioTReC-110-M-005, and BioTReC-111-M-004, respectively.

Author Contributions

C.-H.H., designed and performed experiments, analyzed data and co-wrote the helped paper.; K.-Y.W., J.-P.W. and T.-L.L. performed experiments and analyzed data.; Y.-H.L. provided technology expertise; Z.-S.L. and Y.-H.L. provided essential mouse strains and experimental

knowledge.; P.-W.H. provided essential cell-line strains and experimental knowledge.; Y.-H.L., N.-S.L., and Y.-C.S., provided essential mouse strains.; C.-C.L., K.-H.Y., C.-H.A.Y. and T.-J.C. analyses of the bioinformatics data and co-wrote the paper. Y.-H.L. and N.-S.L. provided technology expertise, ideas and essential materials.; Y.-C.S. and C.-K.J.S. provided ideas, supervised the research and co-wrote the paper.

Funding

This work was supported by Taipei Medical University (to C.-K. J. S.), Academia Sinica (to C.-K. J. S.), Chang-Gung University (CMRPG2J0341 to Y.-C. S.), and MOST grants (NSC 102-2320-B-001-010 to N.-S. L., MOST 103-2311-B-010-003 Y.-C. S., and MOST 110-2628-B-001-024 to L.-Y. C.).

Availability of data and materials

The data that support the findings of this study are available from the corresponding authors upon request.

Material and Methods

Mice

C57BL/6, B6, and FVB mice were purchased from Jackson Laboratories (Bar Harbor, Maine). The B6 *Eklf*(K74R), B6 *Eklf*(K74A) and FVB *Eklf*(K74R) mice were established with the assistance of the Transgenic Core Facility (TCF), IMB, Academia Sinica, Taiwan. As described previously[21], the K74R mutation was introduced by homologous recombination into exon 2 (E2) of the *Eklf* gene of B6 mice by means of a recombinant retrovirus containing the construct loxP-PGK-gb2-neo-loxP-E2 (K74R), before excising the neomycin (neo) selection marker by crossing with Ella-Cre mice. The heterozygous *Eklf*(K74R/+) mice were then crossed to obtain homozygous mutant *Eklf*(K74R/K74R) mice, hereafter termed *Eklf*(K74R) mice.

On the other hand, *Eklf*(K74A) mice were generated by using the CRISPR/Cas9 system. Female B6 mice (7- to 8-week-old) were mated with B6 males and the fertilized embryos were collected from the oviducts. For oligos injection, Cas mRNA (100 ng/μl), sgRNA (50 ng/μl), and donor oligos (100 ng/μl) were mixed and injected into the zygotes at the pronuclei stage. The F0 mice were genotyped by PCR and DNA sequencing. The heterozygous

Eklf(K74A/+) mice were crossed to establish the germ-line stable homozygous *Eklf*(K74A) F1 strain.

Eklf(K74R) mice in the FVB background were generated using an in vitro fertilization strategy. Briefly, sperm from male B6 *Eklf*(K74R) mice was used to fertilize FVB mouse oocytes. In vitro fertilizations of FVB oocytes were carried out consecutively for five generations. The resulting chimeric mice with >90% FVB background were then crossed with FVB mice for another five generations or more.

Cell lines

Murine B16-F10 melanoma cell lines were purchased from ATCC (CRL-6475). B16-F10 cells expressing luciferase (B16-F10-luc) were generated as described previously[61]. All cell lines were derived from cryopreserved stocks split fewer than three times and they were confirmed as mycoplasma-free prior to use. B16-F10 cells were cultured at 37 °C and 5 % CO2 in DMEM medium supplemented with 10 % FBS, 1 % penicillin/streptomycin, and 2 mM L-glutamine. B16-F10-luc cells were selected at 37 °C and 5 % CO2 in a DMEM medium supplemented with 0.2 mg/mL zeocin (Invitrogen), 10 % FBS, 1 % penicillin/streptomycin, and 2 mM L-glutamine.

Experimental melanoma metastasis assay

Cultured B16-F10 melanoma cells ($1x10^5$, $2x10^5$, $5x10^5$ cells/mouse) were injected into mouse tail vein of 8- to 9-week-old or 24-month-old *Eklf*(K74R) and WT mice with/ without bone marrow transplantation. Two weeks after injection, the mice were sacrificed and the number of tumor foci on their lungs was quantified[62].

Flow cytometric analysis and cell sorting

Single cell suspensions of the peripheral blood cells and spleen tissue of B6 mice were prepared by lysing red blood cells and then passing them through a 40-μm cell strainer (Falcon®). Bone marrow mononuclear cells (BMMNCs) were prepared as described below in the section **Bone marrow transplantation (BMT)**. The peripheral blood cells and splenocytes were stained extracellularly for 30 min at room temperature using different combinations of the following antibodies: anti-CD45.1 (eBioscience); anti-CD45.2 (eBioscience); anti-CD3e (eBioscience); anti-CD45R (eBioscience); anti-NK1.1 (eBioscience); anti-PD-1 (eBioscience) and anti-PD-L1 (eBioscience). The various hematopoietic progenitor cell compartments of bone marrow were also stained extracellularly

for 30 min at room temperature by using different combination of the following antibodies: anti-Lineage (eBioscience), anti-c-Kit (eBioscience), anti-Sca-1 (eBioscience), anti-CD34 (eBioscience), anti-Flt-3 (eBioscience). All the immuno-stained cells were subsequently washed with 1% PBS three times and resuspended for FACS analysis and sorting. Small amounts of the cell samples were run on a FACS Analyzer LSRII-12P (BD Bioscience) to determine the proportions of different cell preparations. FACS AriaII SORP (BD Bioscience) was then used to sort the indicated cell populations. The detail gating subsets for all the cell as described above are shown in Table S1. Data analysis was performed using FlowJo software.

The cell population analysis of leukocytes was performed at the Immune Monitoring Core, TMU. The leukocytes of 3- or 24-month-old WT and *Eklf*(K74R) mice were analyzed by flow cytometry to determine the populations of $CD3^+$-$B220^-$-T cells, $CD3^-$- $B220^+$-B cells, $CD3^-$-$NK1.1^+$-NK cells, $CD3^+$-$B220^-$-$CD4^+$ helper T cells (Th), $CD3^+$-$B220^-$-$CD8^+$ cytotoxic T cells (Tc), $CD3^+$-$B220^-$-$CD4^+$-INF-γ^+ (Th1), and $CD3^+$-$B220^-$-$CD4^+$-IL-4^+ (Th2).

RNAi knockdown of *Eklf* mRNA from T cells

CD3+ T cells isolated by sorting were cultured in RPMI 1640 medium for one day for recovery and then transfected with EGFP-plasmid (control), scrambled oligonucleotides (SC control), *Eklf* knockdown oligonucleotide 1 (oligo 1), or *Eklf* knockdown oligonucleotide 2 (oligo 2) in a 96-well plate for 48 h using a LONZA electroporation kit (P3 Primary Cell 4D-NucleofectorTM X Kit) and machine (4D-NucleofectorTM Core Unit). Then the cells were lysed using a PureLink® RNA Mini kit (Life Technologies) and analyzed by RT-qPCR.

RT-qPCR and cell treatment

Total RNA from B cells, T cells, white blood cells (WBC) and total blood from the peripheral blood of *Eklf*(K74R) and WT mice were extracted using a PureLink® RNA Mini kit (Life Technologies). The RNAs were reverse-transcribed by means of oligo-dT primers, Maxima H Minus Reverse Transcriptase (Thermo Scientific™) and SYBR Green reagents (Applied Biosystems). RT-qPCR was performed using a LightCycler® Nano machine (Roche). Gene-specific primers for *Eklf*, *Pd-1*, *Pd-l1*, *Pd-l2,* and *Gapdh* were designed using Vector NTI Advance 9 software according to respective mRNA sequences in the NCBI database (primer sequences are available upon request). Expression levels of mRNAs were normalized to that of endogenous *Gapdh* mRNA.

Western blotting (WB)

We adopted a previously described WB procedure[63]. White blood cells (WBC) of *Eklf*(K74R) and WT B6 mice were collected from RBC lysis buffer-treated peripheral blood. The WBC pellets were lysed in sample buffer and run on SDS-PAGE gels. WB with anti-EKLF (Abcam) and anti-actin (Sigma) antibodies was then used to analyze the levels of EKLF and actin protein.

In vivo bioluminescence imaging

Eklf(K74R) and WT B6 mice were physically restrained and $1x10^5$ B16-F10-luc cells/mouse were intravenously injected into their tail vein. Ten days after melanoma cell inoculation, mice were anesthetized for 5 min and injected intraperitoneally with D-luciferin (300 mg/Kg of body weight). Fifteen minutes after maximum luciferin uptake, the mice were subjected to imaging of the lung and liver regions in an IVIS 50 Bioluminescence imager (Caliper Life Sciences) to determine metastatic burden. The same mice were used the next day as recipients of bone marrow transplantation (BMT) from donor WT or *Eklf*(K74R) mice. Following BMT, bioluminescence imaging was performed on days 0, 10, 17 and 24.

Bone marrow transplantation (BMT)

BMT followed the standard protocol described in Imado *et al.* (2004)[22]. B6, CD45.1 or CD45.2 donor mice were sacrificed and their femurs were removed. Bone marrow cells were harvested by flashing the femurs with RPM I1640 medium (GIBCO) using a 27-gauge needle and syringe. The cells were then incubated at 37 °C for 30 min in murine complement buffer containing antibodies against B cells, T cells and NK cells, washed twice with PBS, and then subjected to Ficoll-Paque PLUS gradient centrifugation to collect bone marrow mononuclear cells (BMMNCs). BMMNCs ($1x10^6$ cells/mouse) from donor mice were injected into the tail veins of recipient B6, CD45.2 or CD45.1 mice that had been exposed to total body γ-irradiation of 10, 5 or 2.5 Gy.

Bead-based multiplex assay of serum cytokines

Serum samples were obtained via submandibular blood collection and allowed to clot in uncoated tubes for two hours at room temperature. The tubes were centrifuged at 6,000 rpm and the supernatants were collected for cytokine analysis by bead-based multiplex assay (MILLIPLEX MAP Mouse High Sensitivity T Cell Panel, Millipore) following the manufacturer protocol[25].

Protein extraction

The cell pellets were resuspended in protein extraction buffer (20 mM HEPES, 0.2% SDS, 1 mM EDTA, 1 mM glycerophosphate, 1 mM Na_3VO_4, and 2.5 mM $Na_4P_2O_7$) with protease inhibitor cocktail (Sigma-Aldrich) and 1 mM phenylmethylsulfonyl fluoride (PMSF). The lysates were further homogenized using a Bioruptor (Diagenode) at 4 °C for 15 min, and then centrifuged at 14,000 × *g* at 4 °C for 20 min. The supernatant was transferred to a new tube before determining protein concentration by means of BCA protein assay (Pierce, Thermo Fisher). Protein aliquots were stored at -30 °C until use.

In-solution digestion

Protein solutions were first diluted with 50 mM ammonium bicarbonate (ABC) and reduced with 5 mM dithiothreitol (DTT, Merck) at 60 °C for 45 min, followed by cysteine-blocking with 10 mM iodoacetamide (IAM, Sigma) at 25°C for 30 min. The samples were then diluted with 25 mM ABC and digested with sequencing-grade modified porcine trypsin (Promega) at 37 °C for 16 h. The peptides were desalted using a homemade C18 microcolumn (SOURCE 15RPC, GE Healthcare) and stored at -30 °C until use.

LC-MS/MS analysis

The desalted peptides were diluted in HPLC buffer A (0.1% formic acid in 30% acetonitrile) and loaded onto a homemade SCX column (0.6 × 5 mm, Luna 5 µm SCX 100 Å, Phenomenex). The eluted peptides were then trapped in a reverse-phase column (Zorbax 300SB-C18, 0.3 × 5 mm; Agilent Technologies), and separated on a homemade column (HydroRP 2.5 µm, 75 µm I.D. × 15 cm with a 15 µm tip) using a multi-step gradient of HPLC buffer B (99.9% acetonitrile/0.1% formic acid) for 90 min with a flow rate of 0.3 µl/min. The LC apparatus was coupled to a 2D linear ion trap mass spectrometer (Orbitrap Elite ETD; Thermo Fisher) operated using Xcalibur 2.2 software (Thermo Fisher). Full-scan MS was performed in the Orbitrap over a range of 400 to 2,000 Da and a resolution of 120,000 at m/z 400. Internal calibration was performed using the ion signal of $[Si(CH_3)_2O]6H^+$ at m/z 536.165365 as lock mass. The 20 data-dependent MS/MS scan events were followed by one MS scan for the 20 most abundant precursor ions in the preview MS scan. The m/z values selected for MS/MS were dynamically excluded for 40 sec with a relative mass window of 10 ppm. The electrospray voltage was set to 2.0 kV, and the temperature of the capillary was set to 200 °C. MS and MS/MS automatic gain control was set to 1,000 ms (full scan) and 200 ms

(MS/MS), or to 3 × 106 ions (full scan) and 3,000 ions (MS/MS), for maximum accumulated time or ions, respectively.

Protein identification

Data analysis was carried out using Proteome Discoverer software (version 1.4, Thermo Fisher Scientific). The MS/MS spectra were searched against the SwissProt database using the Mascot search engine (Matrix Science, version 2.5). For peptide identification, 10 ppm mass tolerance was permitted for intact peptide masses, and 0.5 Da for CID fragment ions with an allowance for two missed cleavages arising from trypsin digestion, oxidized methionine and acetyl (protein N-terminal) as variable modifications, and carbamidomethyl (cysteine) as a static modification. Peptide spectrum matches (PSM) were then filtered based on high confidence and a Mascot search engine ranking of 1 for peptide identification to ensure an overall false discovery rate <0.01. Proteins with single peptide hits were removed from further analysis.

Gene Set Enrichment Analysis

The absolute abundance of each peptide was calculated from respective peak intensity based on the PSM abundance. The protein abundance of each sample was calculated from the sum of the peptide abundance. The abundance data were then background-corrected and normalized according to variance stabilizing transformation by using the function "normalize_vsn" in the R package *DEP*[64]. Differential expression across groups was determined using the function "test_diff" based on protein-wise linear models combined with empirical Bayes statistics. Significantly differentially-expressed proteins were determined according to a P-value threshold of 0.01 and a fold-change (FC) >1.5. To establish functional pathways enriched across groups, normalized data for each pair of compared groups were used to perform Gene Set Enrichment Analysis (GSEA v4.2.0)[65] on selected MSigDB gene sets, including Hallmark (H), curated (C2), and immunologic signature (C7) gene sets, by using the default parameters. Normalized enrichment scores (NES) were used to plot a heatmap in the R package *pheatmap* (v1.0.12).

Statistical analysis

Data are shown as mean ± standard deviation (SD) or standard error of the mean (SEM). Comparisons of data under different experimental conditions were carried out using GraphPad Prism 6.0 software (GraphPad). Each error bar represents SEM unless otherwise

indicated. Significant differences in tumor growth on mouse lungs were assessed by Student's t test. A difference between groups was considered statistically significant when the p value was lower than 0.05.

References

1. Aman Y, Schmauck-Medina T, Hansen M, et al. Autophagy in healthy aging and disease. *Nat Aging*. Aug 2021;1(8):634-650. doi:10.1038/s43587-021-00098-4
2. López-Otín C, Blasco MA, Partridge L, Serrano M, Kroemer G. The hallmarks of aging. *Cell*. Jun 6 2013;153(6):1194-217. doi:10.1016/j.cell.2013.05.039
3. Bashor CJ, Hilton IB, Bandukwala H, Smith DM, Veiseh O. Engineering the next generation of cell-based therapeutics. *Nat Rev Drug Discov*. Sep 2022;21(9):655-675. doi:10.1038/s41573-022-00476-6
4. Fontana L, Partridge L. Promoting health and longevity through diet: from model organisms to humans. *Cell*. Mar 26 2015;161(1):106-118. doi:10.1016/j.cell.2015.02.020
5. Longo VD, Anderson RM. Nutrition, longevity and disease: From molecular mechanisms to interventions. *Cell*. Apr 28 2022;185(9):1455-1470. doi:10.1016/j.cell.2022.04.002
6. Mitchell E, Spencer Chapman M, Williams N, et al. Clonal dynamics of haematopoiesis across the human lifespan. *Nature*. Jun 2022;606(7913):343-350. doi:10.1038/s41586-022-04786-y
7. Pálovics R, Keller A, Schaum N, et al. Molecular hallmarks of heterochronic parabiosis at single-cell resolution. *Nature*. Mar 2022;603(7900):309-314. doi:10.1038/s41586-022-04461-2

572 8. Seita J, Weissman IL. Hematopoietic stem cell: self-renewal versus
573 differentiation. *Wiley Interdiscip Rev Syst Biol Med*. Nov-Dec 2010;2(6):640-53.
574 doi:10.1002/wsbm.86
575 9. Montazersaheb S, Ehsani A, Fathi E, Farahzadi R. Cellular and Molecular
576 Mechanisms Involved in Hematopoietic Stem Cell Aging as a Clinical Prospect. *Oxid*
577 *Med Cell Longev*. 2022;2022:2713483. doi:10.1155/2022/2713483
578 10. Frontelo P, Manwani D, Galdass M, et al. Novel role for EKLF in
579 megakaryocyte lineage commitment. *Blood*. Dec 1 2007;110(12):3871-80.
580 doi:10.1182/blood-2007-03-082065
581 11. Nishizawa M, Chonabayashi K, Nomura M, et al. Epigenetic Variation between
582 Human Induced Pluripotent Stem Cell Lines Is an Indicator of Differentiation
583 Capacity. *Cell Stem Cell*. Sep 1 2016;19(3):341-54. doi:10.1016/j.stem.2016.06.019
584 12. Teruya S, Okamura T, Komai T, et al. Egr2-independent, Klf1-mediated
585 induction of PD-L1 in CD4(+) T cells. *Sci Rep*. May 4 2018;8(1):7021.
586 doi:10.1038/s41598-018-25302-1
587 13. Perkins A, Xu X, Higgs DR, et al. Krüppeling erythropoiesis: an unexpected
588 broad spectrum of human red blood cell disorders due to KLF1 variants. *Blood*. Apr
589 14 2016;127(15):1856-62. doi:10.1182/blood-2016-01-694331
590 14. Neuwirtova R, Fuchs O, Holicka M, et al. Transcription factors Fli1 and EKLF
591 in the differentiation of megakaryocytic and erythroid progenitor in 5q- syndrome and
592 in Diamond-Blackfan anemia. *Ann Hematol*. Jan 2013;92(1):11-8.
593 doi:10.1007/s00277-012-1568-1
594 15. Luo Q, Ma X, Wahl SM, Bieker JJ, Crossley M, Montaner LJ. Activation and
595 repression of interleukin-12 p40 transcription by erythroid Kruppel-like factor in
596 macrophages. *J Biol Chem*. Apr 30 2004;279(18):18451-6.
597 doi:10.1074/jbc.M400320200
598 16. Hung CH, Wang KY, Liou YH, et al. Negative Regulation of the Differentiation
599 of Flk2(-) CD34(-) LSK Hematopoietic Stem Cells by EKLF/KLF1. *Int J Mol Sci*.
600 Nov 10 2020;21(22)doi:10.3390/ijms21228448
601 17. Siatecka M, Bieker JJ. The multifunctional role of EKLF/KLF1 during
602 erythropoiesis. *Blood*. Aug 25 2011;118(8):2044-54.
603 doi:10.1182/blood-2011-03-331371
604 18. Pilon AM, Ajay SS, Kumar SA, et al. Genome-wide ChIP-Seq reveals a
605 dramatic shift in the binding of the transcription factor erythroid Kruppel-like factor

606 during erythrocyte differentiation. *Blood*. Oct 27 2011;118(17):e139-48.
607 doi:10.1182/blood-2011-05-355107
608 19. Tallack MR, Magor GW, Dartigues B, et al. Novel roles for KLF1 in
609 erythropoiesis revealed by mRNA-seq. *Genome Res*. Dec 2012;22(12):2385-98.
610 doi:10.1101/gr.135707.111
611 20. Shyu YC, Lee TL, Chen X, et al. Tight regulation of a timed nuclear import
612 wave of EKLF by PKCθ and FOE during Pro-E to Baso-E transition. *Dev Cell*. Feb
613 24 2014;28(4):409-22. doi:10.1016/j.devcel.2014.01.007
614 21. Shyu YC, Liao PC, Huang TS, et al. Genetic Disruption of KLF1 K74
615 SUMOylation in Hematopoietic System Promotes Healthy Longevity in Mice. *Adv*
616 *Sci (Weinh)*. Sep 2022;9(25):e2201409. doi:10.1002/advs.202201409
617 22. Imado T, Iwasaki T, Kataoka Y, et al. Hepatocyte growth factor preserves
618 graft-versus-leukemia effect and T-cell reconstitution after marrow transplantation.
619 *Blood*. Sep 1 2004;104(5):1542-9. doi:10.1182/blood-2003-12-4309
620 23. Iwai Y, Hamanishi J, Chamoto K, Honjo T. Cancer immunotherapies targeting
621 the PD-1 signaling pathway. *J Biomed Sci*. Apr 4 2017;24(1):26.
622 doi:10.1186/s12929-017-0329-9
623 24. Jiang X, Wang J, Deng X, et al. Role of the tumor microenvironment in
624 PD-L1/PD-1-mediated tumor immune escape. *Mol Cancer*. Jan 15 2019;18(1):10.
625 doi:10.1186/s12943-018-0928-4
626 25. Aira C, Ruiz T, Dixon L, Blome S, Rueda P, Sastre P. Bead-Based Multiplex
627 Assay for the Simultaneous Detection of Antibodies to African Swine Fever Virus
628 and Classical Swine Fever Virus. *Front Vet Sci*. 2019;6:306.
629 doi:10.3389/fvets.2019.00306
630 26. Menees KB, Earls RH, Chung J, et al. Sex- and age-dependent alterations of
631 splenic immune cell profile and NK cell phenotypes and function in C57BL/6J mice.
632 *Immun Ageing*. Jan 8 2021;18(1):3. doi:10.1186/s12979-021-00214-3
633 27. Ul-Haq Z, Naz S, Mesaik MA. Interleukin-4 receptor signaling and its binding
634 mechanism: A therapeutic insight from inhibitors tool box. *Cytokine Growth Factor*
635 *Rev*. Dec 2016;32:3-15. doi:10.1016/j.cytogfr.2016.04.002
636 28. Boccardi V, Westman E, Pelini L, et al. Differential Associations of IL-4 With
637 Hippocampal Subfields in Mild Cognitive Impairment and Alzheimer's Disease.
638 *Front Aging Neurosci*. 2018;10:439. doi:10.3389/fnagi.2018.00439

639 29. Rea IM, Gibson DS, McGilligan V, McNerlan SE, Alexander HD, Ross OA.
640 Age and Age-Related Diseases: Role of Inflammation Triggers and Cytokines. *Front*
641 *Immunol*. 2018;9:586. doi:10.3389/fimmu.2018.00586
642 30. Fabian DK, Fuentealba M, Dönertaş HM, Partridge L, Thornton JM. Functional
643 conservation in genes and pathways linking ageing and immunity. *Immun Ageing*.
644 May 14 2021;18(1):23. doi:10.1186/s12979-021-00232-1
645 31. Yeo EJ. Hypoxia and aging. *Exp Mol Med*. Jun 20 2019;51(6):1-15.
646 doi:10.1038/s12276-019-0233-3
647 32. Zhu X, Chen Z, Shen W, et al. Inflammation, epigenetics, and metabolism
648 converge to cell senescence and ageing: the regulation and intervention. *Signal*
649 *Transduct Target Ther*. Jun 28 2021;6(1):245. doi:10.1038/s41392-021-00646-9
650 33. Hamarsheh S, Groß O, Brummer T, Zeiser R. Immune modulatory effects of
651 oncogenic KRAS in cancer. *Nat Commun*. Oct 28 2020;11(1):5439.
652 doi:10.1038/s41467-020-19288-6
653 34. Ni L, Lu J. Interferon gamma in cancer immunotherapy. *Cancer Med*. Sep
654 2018;7(9):4509-4516. doi:10.1002/cam4.1700
655 35. Principe DR, Doll JA, Bauer J, et al. TGF-β: duality of function between tumor
656 prevention and carcinogenesis. *J Natl Cancer Inst*. Feb 2014;106(2):djt369.
657 doi:10.1093/jnci/djt369
658 36. Zitvogel L, Galluzzi L, Kepp O, Smyth MJ, Kroemer G. Type I interferons in
659 anticancer immunity. *Nat Rev Immunol*. Jul 2015;15(7):405-14. doi:10.1038/nri3845
660 37. Zhao G, Zhu G, Huang Y, et al. IL-6 mediates the signal pathway of
661 JAK-STAT3-VEGF-C promoting growth, invasion and lymphangiogenesis in gastric
662 cancer. *Oncol Rep*. Mar 2016;35(3):1787-95. doi:10.3892/or.2016.4544
663 38. Bin-Jumah MN, Nadeem MS, Gilani SJ, et al. Genes and Longevity of Lifespan.
664 *Int J Mol Sci*. Jan 28 2022;23(3)doi:10.3390/ijms23031499
665 39. Hofmann JW, Zhao X, De Cecco M, et al. Reduced expression of MYC
666 increases longevity and enhances healthspan. *Cell*. Jan 29 2015;160(3):477-88.
667 doi:10.1016/j.cell.2014.12.016
668 40. Ocampo A, Reddy P, Martinez-Redondo P, et al. In Vivo Amelioration of
669 Age-Associated Hallmarks by Partial Reprogramming. *Cell*. Dec 15
670 2016;167(7):1719-1733.e12. doi:10.1016/j.cell.2016.11.052

41. Varady KA, Cienfuegos S, Ezpeleta M, Gabel K. Clinical application of intermittent fasting for weight loss: progress and future directions. *Nat Rev Endocrinol*. May 2022;18(5):309-321. doi:10.1038/s41574-022-00638-x

42. Hifumi T, Yamamoto A, Ato M, et al. Clinical Serum Therapy: Benefits, Cautions, and Potential Applications. *Keio J Med*. Dec 25 2017;66(4):57-64. doi:10.2302/kjm.2016-0017-IR

43. Morgan RA, Gray D, Lomova A, Kohn DB. Hematopoietic Stem Cell Gene Therapy: Progress and Lessons Learned. *Cell Stem Cell*. Nov 2 2017;21(5):574-590. doi:10.1016/j.stem.2017.10.010

44. Giannaccare G, Carnevali A, Senni C, Logozzo L, Scorcia V. Umbilical Cord Blood and Serum for the Treatment of Ocular Diseases: A Comprehensive Review. *Ophthalmol Ther*. Jun 2020;9(2):235-248. doi:10.1007/s40123-020-00239-9

45. Wu SY, Fu T, Jiang YZ, Shao ZM. Natural killer cells in cancer biology and therapy. *Mol Cancer*. Aug 6 2020;19(1):120. doi:10.1186/s12943-020-01238-x

46. Daver N, Wei AH, Pollyea DA, Fathi AT, Vyas P, DiNardo CD. New directions for emerging therapies in acute myeloid leukemia: the next chapter. *Blood Cancer J*. Oct 30 2020;10(10):107. doi:10.1038/s41408-020-00376-1

47. Mora J. Autologous Stem-Cell Transplantation for High-Risk Neuroblastoma: Historical and Critical Review. *Cancers (Basel)*. May 24 2022;14(11)doi:10.3390/cancers14112572

48. Conboy IM, Conboy MJ, Wagers AJ, Girma ER, Weissman IL, Rando TA. Rejuvenation of aged progenitor cells by exposure to a young systemic environment. *Nature*. Feb 17 2005;433(7027):760-4. doi:10.1038/nature03260

49. Das MM, Godoy M, Chen S, et al. Young bone marrow transplantation preserves learning and memory in old mice. *Commun Biol*. 2019;2:73. doi:10.1038/s42003-019-0298-5

50. Goodell MA, Rando TA. Stem cells and healthy aging. *Science*. Dec 4 2015;350(6265):1199-204. doi:10.1126/science.aab3388

51. Kang S, Moser VA, Svendsen CN, Goodridge HS. Rejuvenating the blood and bone marrow to slow aging-associated cognitive decline and Alzheimer's disease. *Commun Biol*. Feb 13 2020;3(1):69. doi:10.1038/s42003-020-0797-4

52. Castellano JM, Mosher KI, Abbey RJ, et al. Human umbilical cord plasma proteins revitalize hippocampal function in aged mice. *Nature*. Apr 27 2017;544(7651):488-492. doi:10.1038/nature22067

53. Mehdipour M, Skinner C, Wong N, et al. Rejuvenation of three germ layers tissues by exchanging old blood plasma with saline-albumin. *Aging (Albany NY)*. May 30 2020;12(10):8790-8819. doi:10.18632/aging.103418

54. Siatecka M, Xue L, Bieker JJ. Sumoylation of EKLF promotes transcriptional repression and is involved in inhibition of megakaryopoiesis. *Mol Cell Biol*. Dec 2007;27(24):8547-60. doi:10.1128/mcb.00589-07

55. Aunan JR, Cho WC, Søreide K. The Biology of Aging and Cancer: A Brief Overview of Shared and Divergent Molecular Hallmarks. *Aging Dis*. Oct 2017;8(5):628-642. doi:10.14336/ad.2017.0103

56. Lages CS, Lewkowich I, Sproles A, Wills-Karp M, Chougnet C. Partial restoration of T-cell function in aged mice by in vitro blockade of the PD-1/PD-L1 pathway. *Aging Cell*. Oct 2010;9(5):785-98. doi:10.1111/j.1474-9726.2010.00611.x

57. Schaum N, Lehallier B, Hahn O, et al. Ageing hallmarks exhibit organ-specific temporal signatures. *Nature*. Jul 2020;583(7817):596-602. doi:10.1038/s41586-020-2499-y

58. Aira C, Ruiz T, Dixon L, Blome S, Rueda P, Sastre P. Bead-Based Multiplex Assay for the Simultaneous Detection of Antibodies to African Swine Fever Virus and Classical Swine Fever Virus. Original Research. *Frontiers in Veterinary Science*. 2019-September-13 2019;6doi:10.3389/fvets.2019.00306

59. Zhou J, Zhu Z, Bai C, Sun H, Wang X. Proteomic profiling of lymphocytes in autoimmunity, inflammation and cancer. *J Transl Med*. Jan 7 2014;12:6. doi:10.1186/1479-5876-12-6

60. Zhang D, Chen G, Manwani D, et al. Neutrophil ageing is regulated by the microbiome. *Nature*. Sep 24 2015;525(7570):528-32. doi:10.1038/nature15367

61. Tsai CH, Tzeng SF, Chao TK, et al. Metastatic Progression of Prostate Cancer Is Mediated by Autonomous Binding of Galectin-4-O-Glycan to Cancer Cells. *Cancer Res*. Oct 1 2016;76(19):5756-5767. doi:10.1158/0008-5472.Can-16-0641

62. Narasimhan PB, Eggert T, Zhu YP, et al. Patrolling Monocytes Control NK Cell Expression of Activating and Stimulatory Receptors to Curtail Lung Metastases. *J Immunol*. Jan 1 2020;204(1):192-198. doi:10.4049/jimmunol.1900998

63. Green MR, Sambrook J. *Molecular Cloning: A Laboratory Manual*. Cold Spring Harbor Laboratory Press; 2012.

64. Zhang X, Smits AH, van Tilburg GB, Ovaa H, Huber W, Vermeulen M. Proteome-wide identification of ubiquitin interactions using UbIA-MS. *Nat Protoc*. Mar 2018;13(3):530-550. doi:10.1038/nprot.2017.147

65. Subramanian A, Tamayo P, Mootha VK, et al. Gene set enrichment analysis: a knowledge-based approach for interpreting genome-wide expression profiles. *Proc Natl Acad Sci U S A*. Oct 25 2005;102(43):15545-50. doi:10.1073/pnas.0506580102

Figure Legends

Figure 1. Anti-cancer capability of *Eklf*(K74R) mice as analyzed by the experimental melanoma metastasis assay.

(A) Flow chart illustrating the strategy of the pulmonary tumor foci assay. Left panels, representative photographs of pulmonary metastatic foci on the lungs of WT and *Eklf*(K74R) male mice in the B6 background two weeks after intravenous injection of B16-F10 cells (10^5 cells/ mouse). Statistical comparison of the numbers of pulmonary foci is shown in the two histograms on the right. N=10 (male) and N=7 (female), **, $p<0.01$. Note that only the numbers of large pulmonary foci (>1mm diameter) were scored. N>6, **, $p<0.01$. (B) Pulmonary tumor foci assay of 24-month-old WT and *Eklf*(K74R) male mice. Statistical comparison is shown in the two histograms. N=10

(male), *, $p<0.05$. (C) Pulmonary tumor foci assay of male mice in the FVB background. Statistical comparison is shown in the histograph on the right. N=10, **, $p<0.01$. (D) Pulmonary tumor foci assay of *Eklf*(K74A) male mice. Statistical comparison of the 3-month-old WT and *Eklf*(K74A) mice numbers of pulmonary foci is shown in the two histograms. N=10 (male), **, $p<0.01$.

Figure 2. Transfer of cancer resistance of *Eklf*(K74R) mice to WT mice by bone marrow transplantation (BMT)

(A) Flow chart illustrating the experimental strategy. (B) FACS analysis of the efficiency of BMT with use of 10Gy γ-irradiation. The percentages of CD45.1/CD45.2 cells in the PB of the recipient male mice were analyzed by flow cytometry, with the representative FACS charts shown on the left and the statistical histobar diagram on the right. (C) Transfer of the anti-metastasis capability of 8-week-old *Eklf*(K74R) male mice to age-equivalent WT male mice by BMT with use of 10Gy γ-irradiation. Left panels, representative photographs of lungs with pulmonary metastatic foci in the recipient WT (CD45.1) mice after BMT from WT (CD45.2) or *Eklf*(K74R) (CD45.2) donor mice and challenged with B16-F10 cells. Statistical analysis of the numbers of pulmonary B16-F10 metastatic foci on the lungs is shown in the right histogram. n=10, *, $p<0.05$. (D) Transplantation of 8-week-old male WT (CD45.1) mice with BMMNC from age-equivalent WT (CD45.2) male mice or from *Eklf*(K74R) (CD45.2) male mice with use of the γ-irradiation dosage 2.5Gy or 5Gy. The histobar diagram comparing the percentages of CD45.1 and CD45.2 PB cells of the recipient WT mice after BMT is shown on the left. The statistical analysis of the average numbers of pulmonary foci on the lungs of recipient WT mice after BMT and injected with the B16-F10 cells is shown in the right histogram, N=6. **, $p<0.01$, ***, $p<0.001$.

Figure 3. Inhibition of tumor growth in WT mice by BMT from *Eklf*(K74R) mice

(A) A flow chart of the experiments. Luciferase-positive B16-F10 cells were injected into the tail vein of 8-week-old WT male mice (day 0). The mice were then transplanted with BMMNC from WT or *Eklf*(K74R) male mice on day 11 after the luciferase-positive B16-F10 cell injection. *In vivo* imaging system (IVIS) was used to follow the tumor growth in mice on day 0, 10, 17 and 24, respectively. (B) Representative images of bioluminescence reflecting the luciferase activity from melanoma cancer cells in mice. The color bar indicates the scale of the

797 bioluminescence intensity. (C) Statistical analysis of the intensities of bioluminescence
798 in the cancer-bearing mice (WT→WT, purple, N=7; *Eklf*(K74R)→WT, blue, N=8;
799 Control (no BMT), red, N=3).
800
801 **Figure 4. Decrease of *Pd-1* and *Pd-l1* expression in blood cells of *Eklf*(K74R) mice**
802 (A) Levels of *Pd-1* and *Pd-l1* mRNAs in the PB of WT and *Eklf*(K74R) male mice at
803 the ages of 3 months and 24 months, respectively, as analyzed by RT-qPCR. Note the
804 relatively low levels of *Pd-1* and *Pd-l1* mRNAs in the *Eklf*(K74R) mice at both ages in
805 comparison to the WT mice. (B) Upper panels, comparison of the mRNA levels of
806 *Pd-1* and *Pd-l1* of $CD3^+$ T cells and $B220^+$ B cells isolated from the PB of 8-week-old
807 WT and *Eklf*(K74R) male mice. N=5. *, $p<0.05$; **, $p<0.01$. Lower panels, comparison
808 of the protein levels of PD-1 and PD-L1, as analyzed by flow cytometry, of $CD3^+$ T
809 cells and $B220^+$ B cells from 8-week-old WT and *Eklf*(K74R) male mice. N=3. *,
810 $p<0.05$; **, $p<0.01$. (C) Comparison of the levels of *Pd-1, Pd-l1* and *Eklf* mRNAs, as
811 analyzed by RT-qPCR, in $CD3^+$ T cells, which were isolated from splenocytes, without
812 or with RNAi knockdown of *Eklf* mRNA. Two oligos (oligo-1 and oligo-2) were used
813 to knockdown *Eklf* mRNA by ~60-70%, which resulted in the reduction of *Pd-1*
814 mRNA level by 30-60% and nearly complete depletion of *Pd-l1* mRNA. Control, T
815 cells transfected with GFP-plasmid. SC, T cells transfected with scrambled oligos. N>3.
816 *, $p<0.05$; **, $p<0.01$; ***, $p<0.001$.
817
818

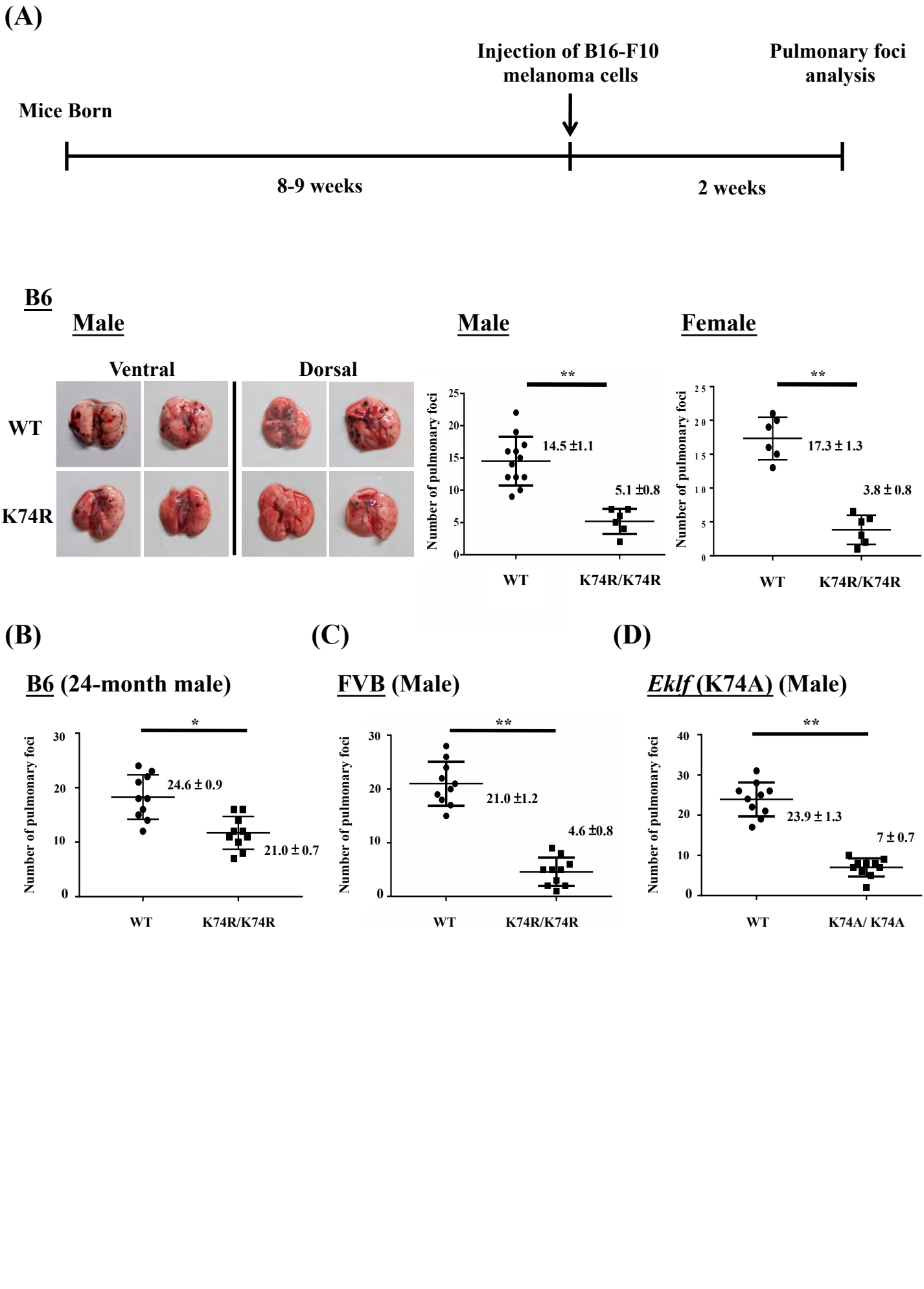

Fig. 2

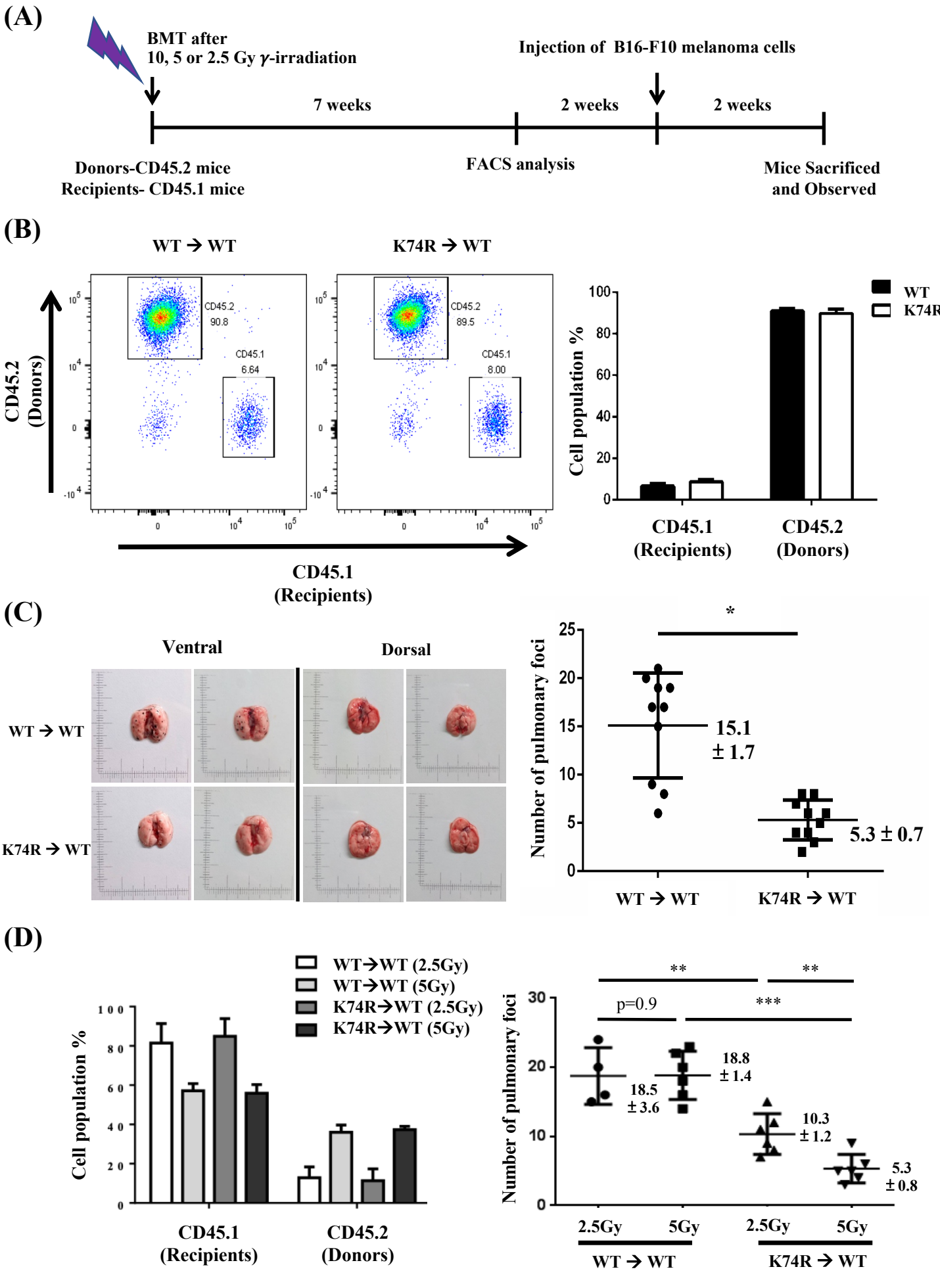

Fig. 3

(A)

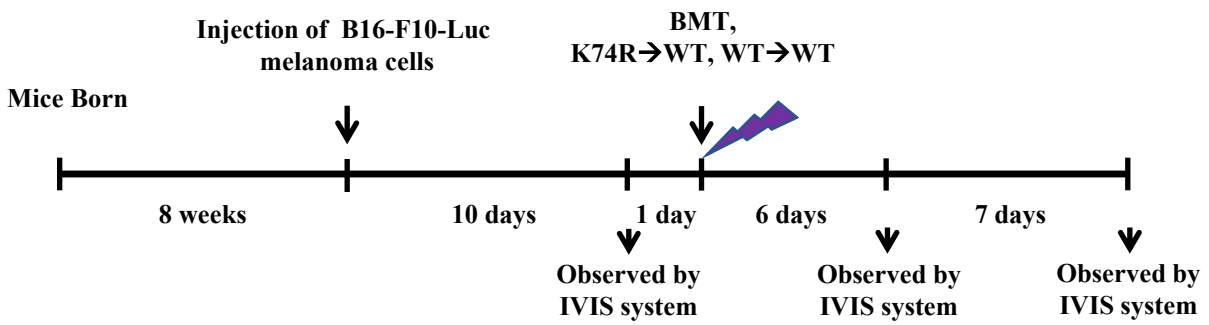

(B)

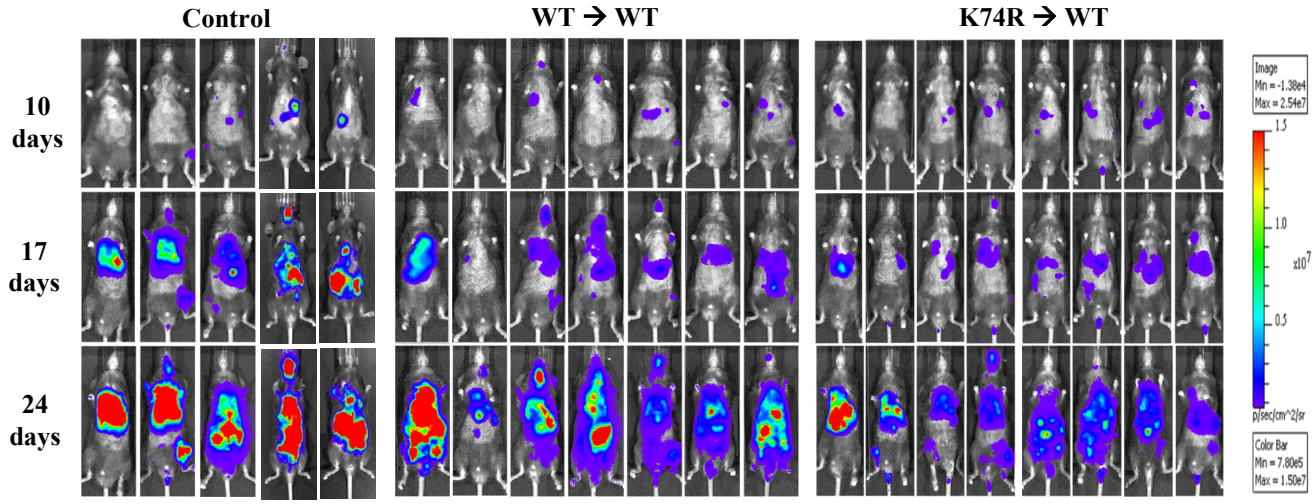

(C)

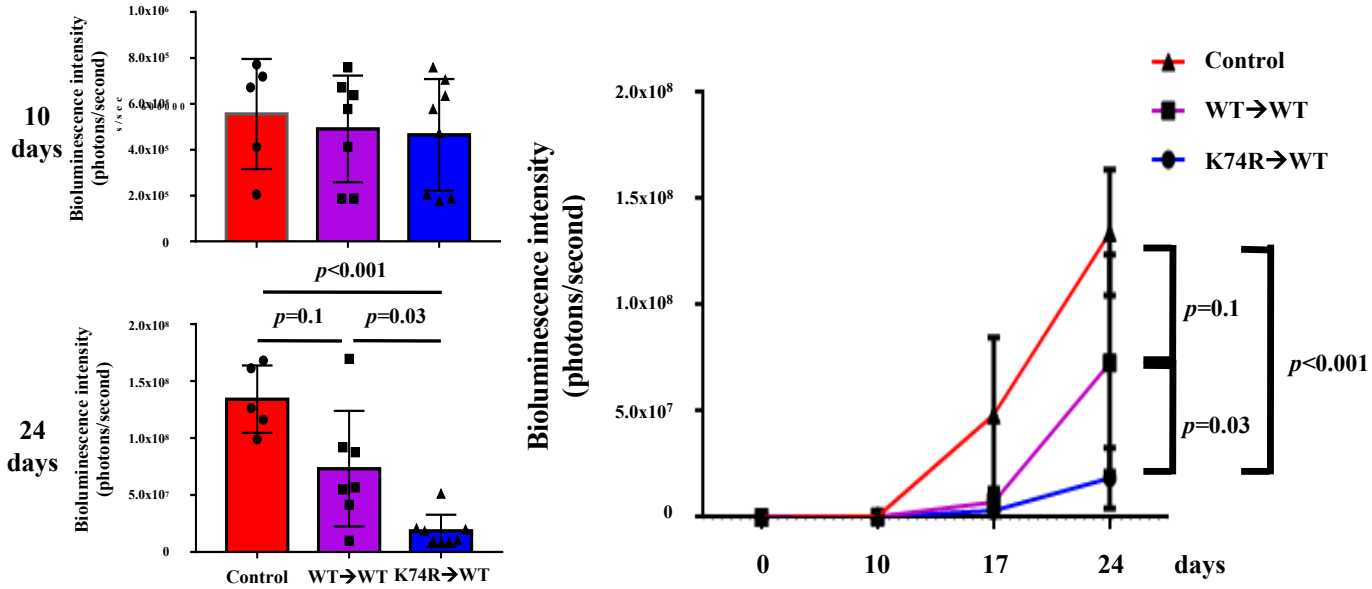

Fig. 4